17th World Conference on Earthquake Engineering, 17WCEE
Sendai, Japan - September 13th to 18th 2020

TIME-FREQUENCY REPRESENTATION MODEL FOR SEISMIC GROUND MOTIONS

X.Z. Cui[1], H.P. Hong[2]

[1] *Ph.D. candidate, Department of Civil and Environmental Engineering, the University of Western Ontario, London, Ontario, Canada, xcui55@uwo.ca*
[2] *Professor, Department of Civil and Environmental Engineering, the University of Western Ontario, London, Ontario, Canada, hongh@eng.uwo.ca*

Abstract

Models to simulate ground motions that take into account their nonstationarity are widely used. Many of these models are based on the evolutionary spectral theory. In particular, the amplitude modulated evolutionary stochastic process defined by the evolutionary power spectral density (EPSD) function is a very popular model. Seismic ground motions and the ground motion simulation can be carried out using the spectral representation method. Such a model neglects possible frequency modulation observed from actual ground motions. In the present study, a procedure to develop time-frequency PSD (TFPSD) function of ground motions is proposed based on the S-transform. The use of the S-transform provides frequency-dependent resolution with absolutely referenced phase information. The application of the proposed procedure leads to a probabilistic TFPSD model for scenario seismic events. The use of the procedure is given by considering more than 1500 far-field ground motion records of strike-slip fault earthquakes. The procedure includes the identification and estimation of the model parameters for the TFPSD model as functions of earthquake magnitude, rupture distance and shear wave velocity at the site. Sets of ground-motion models for a set of model parameters are developed and suggested.

Keywords: Seismic ground motions, time-frequency representation, S-transform, discrete orthonormal S-transform, simulation.

1. Introduction

The seismic risk assessment for a given scenario event could be assessed based on its ground motion measures or corresponding time-history ground motions. The ground motion measures can be predicted using the ground motion models that are developed based on instrumental ground-motion data from past earthquakes such as those reported in NGA-West2 GMMs [1~4]. The ground motion measures include the peak ground acceleration, peak ground velocity, and spectral acceleration. However, in some cases, the use of the time-history ground motions for seismic risk analysis can be valuable and advantageous [5]. Such modelling and simulation of the time histories of the ground motion could be carried out based on the stochastic point source model or finite fault model [6,7]. The model requires the use of a set of well-calibrated model parameters as well as a time-dependent amplitude modulated function. In essence, these models represent the ground motions as evolutionary stochastic processes [8,9]. However, the modeling often only considers the amplitude modulation and possible frequency modulation observed from actual ground motions [11,12] is neglected.

Alamilla et al. developed a probabilistic model for the evolutionary stochastic process based on ground motion records applicable to Mexico [13]. Their model considers both the amplitude as well as frequency modulation functions. The time-history ground motions based on this model can be simulated based on the spectral representation method (SRM) [14]. Other models that consider time-varying amplitude and frequency of the ground motion measures include those developed in [15~19].

The TFPSD function given in [15,16] was developed based on the time-frequency representation of ground motion records by applying the short-time Fourier transform (STFT). The model developed in [17,18] was based on the consideration that the ground motion could be represented by filtering the white-noise through a response function with time-varying parameters. The model reported in [19] was based on the wavelet packets modelling. The inadequacy of the application of STFT that partitions the nonstationary signal into blocks of equal length is well-known in the literature [20,21]. This includes the resolution in time and frequency plane and the energy leakage. The problem could be overcome by carrying out time-frequency representation analysis using the S-transform [22]. The use of the S-transform provides frequency-dependent resolution with absolutely referenced phase information

In the present study, some preliminary analysis results leading to a probabilistic TFPSD model of the ground motions are presented. The model depends on the seismic event parameters and is developed based on actual ground motion records obtained from the NGA-West2 database for the strike-slip fault earthquakes. For the evaluation of the TFPSD function of the ground motion, the S-transform is employed. Regression analysis is carried out to identify the model parameters. The developed model is described in the following sections.

2. Selected ground motion database

Ground motion records for the strike-slip fault type of events were selected from the NGA-West2 database [23]. Three commonly used parameters describing the earthquake events (M, R_{rup} and V_{S30}) for engineering applications are considered for the selection of records in the present study, where M represents the moment magnitude; R_{rup} represents the closest distance from the recording site to the fault area, and V_{S30} represents the shear-wave velocity for the top 30m of the site soil. The selection is based on the following criteria:

1). M is greater than 4.5 and R_{rup} is between 10 and 300 km so to exclude the near-fault records and low-intensity records;

2) V_{S30} between 180 m/s and 1500 m/s is considered to consider the site Class B, C and D only [24];

3) The records from aftershocks or records without the necessary information are not considered;

4) Only records from strike-slip fault earthquakes are included;

5) Records are inspected and baseline correction is considered; and

6) Each event should contain at least five pairs of records so assessment of the inter- and intra-event effects may be carried out.

According to the above criteria, 1504 pairs of records, each with two horizontal components, are selected from 35 events and are used in this study. The distribution of M and R_{rup} associated with the selected records and the number of records with different site classes [24] are shown in Fig. 1.

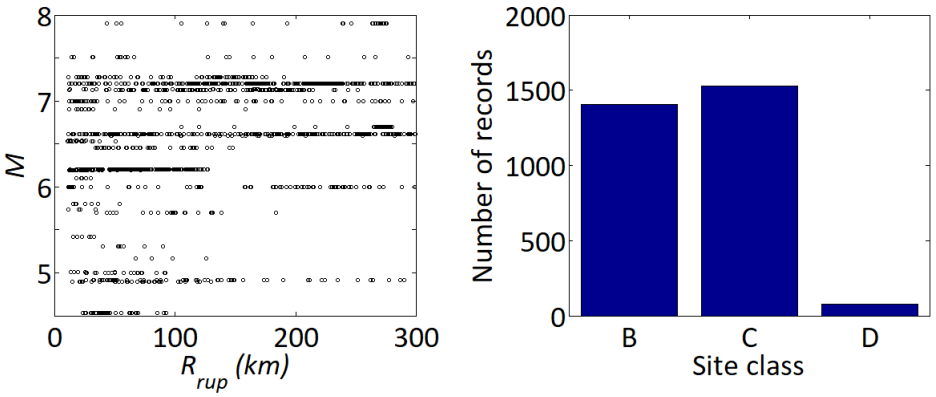

Fig. 1 – M and R_{rup} distribution of selected records (left) and the number of selected records for each site class (right)

3. Time-frequency representation of seismic ground motions through S-transform

To assess the time-frequency representation of the ground motion record, $x(t)$, the S-transform is applied. This transform for $x(t)$, $t \in [0,T]$, can be written as [22,25],

$$x_S(f,t) = \int_0^T x(\tau) w(f, t-\tau) e^{-i2\pi f\tau} d\tau \tag{1}$$

where $x_S(f,t)$ denotes the S-transform coefficients, f is the frequency as in the Fourier transform, and t is the center of the window function $w(f,t-\tau)$ defined as,

$$w(f,t-\tau) = \frac{|f|}{\sqrt{2\pi}\kappa} \exp\left(-\frac{f^2(t-\tau)^2}{2\kappa^2}\right) \tag{2}$$

where κ is a parameter controlling the effective width of the window. The double-sided Time-frequency power spectral density (TFPSD) function, $S_{Sx}(f,t)$, can be defined as [26],

$$S_{Sx}(f,t) = \frac{x_S(f,t)[x_S(f,t)]^*}{D_\kappa |f|} \tag{3}$$

where D_k is a constant that can be evaluated numerically and is very close to $1/\sqrt{4\pi\kappa^2}$, and the superscript * denotes the complex conjugate. This definition ensures energy conservation. Models to simulate the nonstationary stochastic ground motions defined by $S_{Sx}(f,t)$ were developed in [26,27]. The single-sided TFPSD function equals twice of the double-sided TFPSD function. In the remaining part of this study, unless otherwise indicated, the single-sided TFPSD function is considered, and the same symbol $S_{Sx}(f,t)$ is used to denote the single-sided TFPSD function.

To develop a probabilistic model of $S_{sx}(f,t)$ based on a set of ground motion records, first, the normalized TFPSD function $S_{sx}(f,t)$, denoted as $S_{0sx}(f,t)$, is evaluated for each record component:

$$S_{0sx}(f,t) = S_{sx}(f,t) / E_T \tag{4}$$

where $E_T = \int_0^{+\infty}\int_0^T S_{sx}(f,t)dtdf$ is the total energy. An illustration of the calculated $S_{0sx}(f,t)$ for a selected record is shown in Fig. 2. Also shown in the figure are the total energy E_T, the PSD function (i.e., integral of $S_{sx}(f,t)$ over the time), and the time-varying envelop function $A(t)$, which is defined as the integral of $S_{sx}(f,t)$ over f.

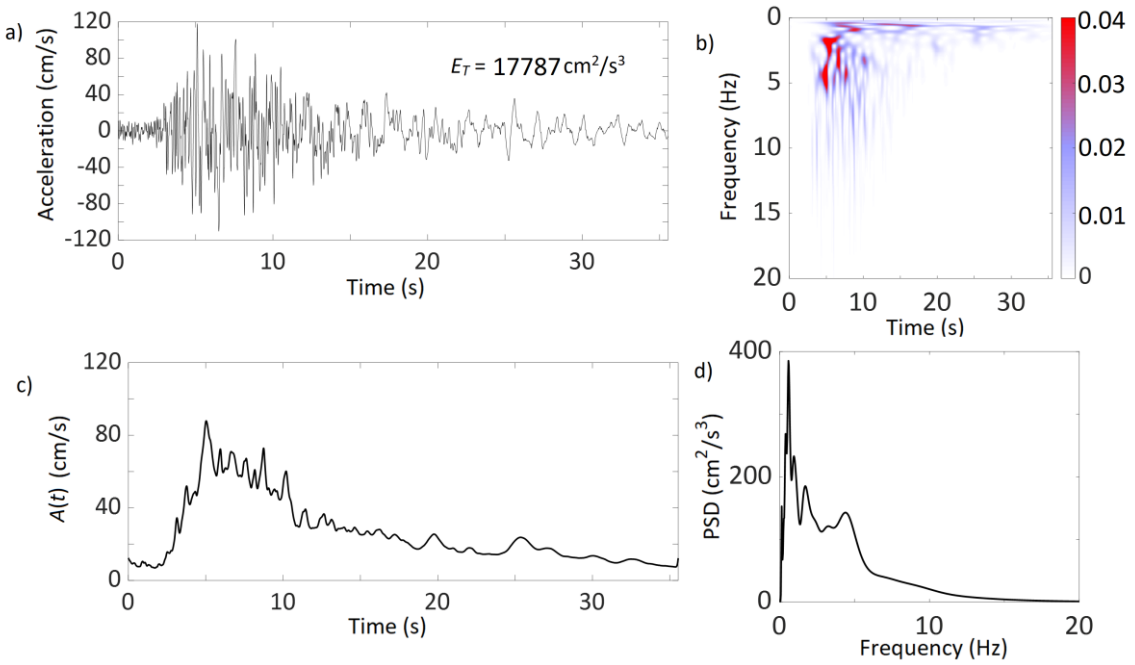

Fig. 2 – a) A selected record; b) normalized TFPSD function; c) time-varying envelop function $A(t)$; and d) PSD function.

By carrying out the analysis as shown in Fig. 2 for each horizontal record component, sets of quantities, E_T, $S_{0sx}(f,t)$ and $A(t)$ are obtained. To develop the probabilistic model, similar to [15], the calculation is carried out for the following quantity for each record component,

$$\begin{aligned} P_a(t) &= \lambda_0(t) \\ F_c(t) &= \lambda_1(t) / \lambda_0(t) \\ F_b(t) &= [\lambda_2(t) / \lambda_0(t) - F_c^2(t)]^{1/2} \end{aligned} \tag{5}$$

but based on the TFPSD function obtained from the S-transform, where $\lambda_i(t)$ is the i-th moment of $S_{0sx}(f,t)$ (i.e., $\lambda_i(t) = \int f^i S_{0sx}(f,t)df$ $i = 0,1,2;$); $F_c(t)$ and $F_b(t)$ are the central frequency and the frequency bandwidth of $S_{0sx}(f,t)$ at time t, respectively; $P_a(t)$ is the normalized energy distribution in time. Based on the above, $A(t) = \sqrt{E_T P_a(t)}$. Consequently, the Arias intensity normalized with respect to E_T, $I_{0A}(t)$, is given by,

$$I_{0A}(t) = \int_0^t P_a(\tau) d\tau \tag{6}$$

An illustrated of the calculated $P_a(t)$, $F_c(t)$, $F_b(t)$ and $I_{0A}(t)$ of the record shown in Fig. 2 is presented in Figure 3.

By considering that the energy distributed in frequency at a given time can be represented using the mathematical function that is the same as the lognormal distribution density function, $S_{0\mathcal{S}x}(f,t)$, is then represented as,

$$S_{0\mathcal{S}x}(f,t) = \frac{P_a(t)}{f\sqrt{2\pi\delta(t)}} \exp\left[-\frac{1}{2}\left(\frac{\ln f - \ln\beta(t)}{\delta(t)}\right)^2\right] \tag{7}$$

where $\delta(t)$ and $\beta(t)$ are calculated using,

$$\begin{aligned} \delta(t) &= \sqrt{\ln[1 + F_b^2(t)/F_c^2(t)]} \\ \ln\beta(t) &= \ln F_c(t) - \delta^2(t)/2 \end{aligned} \tag{8}$$

In Eq. (8), $\delta(t)$ is time-dependent which is unlike the model given by [15], where $\delta(t)$ is treated as a constant. The parameters $\delta(t)$, $\beta(t)$ and $P_a(t)$ define the time-frequency variation of the energy of the stochastic process.

To fit a parametric model to $P_a(t)$ or its integrated version $I_{0A}(t)$, it is considered that $P_a(t)$ follows the mathematical form defined by the Johnson SB distribution. That is, $I_{0A}(t)$ could be modelled by the mathematical form defined by the Johnson SB distribution. This results in,

$$I_{0A}(t) = \Phi\left(\gamma + \delta \ln\left(\frac{t/T}{1-t/T}\right)\right), \quad t \in [0,T] \tag{9}$$

where $\Phi(\bullet)$ is the cumulative normal distribution function, γ and δ are the parameters to control the shape and T is the duration. Based on the relation between $I_{0A}(t)$ and $P_a(t)$, $P_a(t)$ is modelled by the following equation:

$$P_a(t) = \frac{\delta T}{\sqrt{2\pi} t(T-t)} \exp\left[-\frac{1}{2}\left(\gamma + \delta \ln\frac{t/T}{1-t/T}\right)^2\right] \tag{10}$$

Regression analysis can be carried out based on the assumed model to find the model parameters. An illustration of such a fitting is shown in Fig. 3a and 3b. From the fitted model, one could find the time, t_{Peak}, where $P_a(t)$ attains its maximum, and the time t_p where the normalized accumulation of energy $I_{0A}(t)$ equals p. It is noted that the effective duration of the ground motions (e.g. $D_{0.05\sim0.95} = t_{0.95} - t_{0.05}$, the time interval between times at 5% and 95% of the Arias intensities), is often used in the literature [28]. By considering such an interval, the model parameters γ and δ can be related to t_{Peak}, $t_{0.05}$, and $D_{0.05\sim0.95}$ as follows,

$$\delta = \left[\Phi^{-1}(0.95) - \Phi^{-1}(0.05)\right] / \ln\left[\frac{t_{0.05} + D_{0.05\sim0.95}}{T - t_{0.05} - D_{0.05\sim0.95}} \frac{T - t_{0.05}}{t_{0.05}}\right]$$
$$\gamma = -1 - \delta \ln\left[\frac{t_{Peak}}{T - t_{Peak}}\right] \quad (11)$$

where $\Phi^{-1}(\bullet)$ is the normal inverse cumulative distribution function. The first expression in Eq. (11) is based on the spread of the energy, while the second one is based on the occurrence of maximum $P_a(t)$. A preliminary analysis indicates that γ and δ for all considered records do not follow very clear trends for ranges of magnitude, rupture distance and shear wave velocity values. Therefore, rather than develop empirical relations for γ and δ, empirical equations for t_{Peak}, $t_{0.05}$, and $D_{0.05\sim0.95}$ as functions of magnitude, rupture distance and shear wave velocity are to be developed as described in the following.

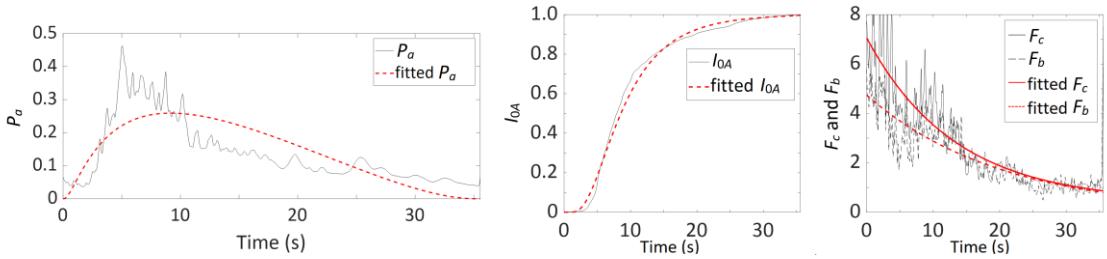

Fig. 3 – $I_{0A}(t)$, $P_a(t)$, $F_c(t)$ and $F_b(t)$ and their fitted curves.

Based on a preliminary analysis of the records, it is observed that in general, $F_c(t)$ and $F_b(t)$ decrease with exponential decay. Their decay is more pronounced at the beginning of the ground motions and becomes more stable as time increases. Moreover, $F_c(t)$ and $F_b(t)$ could be approximated by the exponential decay forms,

$$F_c(t) = a\exp[-bt/T] + c$$
$$F_b(t) = d\exp[-et/T] + g \quad (12)$$

where a, b, c d, e, and g are the model parameters. These model parameters can be obtained based on regression analysis. An example analysis result is presented in Fig. 3c. Using the fitted models, the values of $F_c(t)$ at t = 0, T/2 and T, denoted as $F_{c,0}$, $F_{c,T/2}$ and $F_{c,T}$, and the values of $F_b(t)$ at t = 0, T/2 and T denoted as $F_{b,0}$, $F_{b,T/2}$ and $F_{b,T}$, can be calculated. Alternatively, given values of $F_{c,0}$, $F_{c,T/2}$, $F_{c,T}$, $F_{b,0}$, $F_{b,T/2}$ and $F_{b,T}$. a, b, c d, e, and g can be calculated. Since a preliminary analysis indicates that empirical equations for $F_{c,0}$, $F_{c,T/2}$, $F_{c,T}$, $F_{b,0}$, $F_{b,T/2}$ and $F_{b,T}$ as functions of magnitude, rupture distance and shear wave velocity are associated with less scatters than those for a, b, c d, e, and g, in the following the empirical equations are developed for $F_{c,0}$, $F_{c,T/2}$, $F_{c,T}$, $F_{b,0}$, $F_{b,T/2}$ and $F_{b,T}$.

4. Regression analysis results

By repeating the analysis described in the previous section for each record component, the 11 parameters (e.g. $\ln(E_T)$, T, $D_{0.05\sim0.95}$, t_{Peak}, $t_{0.05}$, $F_{c,0}$, $F_{c,T/2}$, $F_{c,T}$, $F_{b,0}$, $F_{b,T/2}$ and $F_{b,T}$) are calculated for each record component. Using $\ln(E_T)$ instead of E_T is due to that the total energy of an earthquake usually follows a lognormal distribution. To better characterize $D_{0.05\sim0.95}$ in a nondimensional form, a ratio $r_D = D_{0.05\sim0.95}/T$ instead of $D_{0.05\sim0.95}$ is used. Similarly, instead of t_{Peak} and $t_{0.05}$, the ratios $r_{t_{Peak}} = (t_{Peak} - t_{0.05})/D_{0.05\sim0.95}$ and

$r_{t_{0.05}} = t_{0.05} / (T - t_{0.95})$ are used. $r_{t_{Peak}}$ represent the relative location of t_{Peak} in the time interval $D_{0.05\sim0.95}$ and $r_{t_{0.05}}$ represent the ratio between the time of Arias intensities below 5% and the time of Arias intensities from 95% to 100%. r_D and $r_{t_{Peak}}$ are bounded between 0 and 1 and $r_{t_{0.05}}$ is always positive. Regression analysis is carried out for the 11 parameters (e.g. **P**=[ln(E_T), T, r_D, $r_{t_{Peak}}$, $r_{t_{0.05}}$, $F_{c,0}$, $F_{c,T/2}$, $F_{c,T}$, $F_{b,0}$, $F_{b,T/2}$ and $F_{b,T}$]) by considering all samples from the considered records.

First, statistical analysis and distribution fitting is carried out for the considered model parameters. The fitted distributions are shown in Figure 4. It can be observed that not all of them are normally distributed or approximately normally distributed.

To carry out regression analysis, a mapping of the variables to normal space is carried out using,

$$z_i = \Phi^{-1}[F_i(P_i)] \tag{13}$$

where P_i is the i-th element of **P**; $F_i(\bullet)$ represents the cumulative probability distribution of variable P_i and $\Phi^{-1}[\bullet]$ is the inverse of the cumulative normal distribution function; and z_i is the standard normally distributed random. In the normal space, the regression analysis is carried out, resulting in:

$$\begin{aligned}
z_1 &= 23.12 + 29.88M - 1.19M^2 - 86.90\ln M - 0.95\ln R_{rup} + \varepsilon_1 \\
z_2 &= -2.08 + 0.61\ln R_{rup} - 0.12\ln V_{S30} + \varepsilon_2 \\
z_3 &= -85.01 - 93.62M + 3.80M^2 + 284.23\ln M + 0.16\ln R_{rup} + \varepsilon_3 \\
z_4 &= 16.07 + 25.81M - 1.08M^2 - 73.71\ln M + \varepsilon_4 \\
z_5 &= -34.63 - 38.00M + 1.55M^2 + 115.3\ln M + \varepsilon_5 \\
z_6 &= -2.35 - 0.006M^2 - 0.03R_{rup} + 1.23\ln R_{rup} + \varepsilon_6 \\
z_7 &= 43.66 + 42.57M - 1.69M^2 - 132.62\ln M - 0.006R_{rup} + \varepsilon_7 \\
z_8 &= 31.23 + 26.78M - 1.05M^2 - 86.20\ln M + \varepsilon_8 \\
z_9 &= -2.56 + 0.004M^2 - 0.03R_{rup} + 1.15\ln R_{rup} + \varepsilon_9 \\
z_{10} &= 64.32 + 68.15M - 2.73M^2 - 208.91\ln M - 0.006R_{rup} + \varepsilon_{10} \\
z_{11} &= 57.44 + 58.17M - 2.31M^2 - 180.23\ln M - 0.006R_{rup} + \varepsilon_{11}
\end{aligned} \tag{14}$$

where ε_i represents the residual which includes both the inter- and intra- event effects (denoted as η_i and δ_i). For the preliminary analysis, a separate treatment of η_i and δ_i as well as the correlation among the model parameters are not considered. These regression equations are obtained by the trial and error approach. The models depend on M, R_{rup} and V_{S30}. There are significant scatters, and the scatter depend on M, R_{rup} and V_{S30}. The investigation of such a dependency, as well as the models for η_i and δ_i, is the subject of our ongoing research. It is found that the magnitude and rupture distance influence significantly the 11 model parameters; the impact of the shear wave velocity on the model parameter is less pronounced. An illustration of the dependency of the model parameters to M and R_{rup} is illustrated in Figure 5. These plots indicate that the selected model in Eq. (14) can represent the variation of these parameters in terms of M and R_{rup}.

Note that given the model parameters shown in Eq. (14), the model parameters **P**=[ln(E_T), T, r_D, $r_{t_{Peak}}$, $r_{t_{0.05}}$, $F_{c,0}$, $F_{c,T/2}$, $F_{c,T}$, $F_{b,0}$, $F_{b,T/2}$ and $F_{b,T}$]) can be calculated using $P_i = F_i^{-1}\Phi(z_i)$. These parameters can then be used to define the TFPSD function $S_{\mathcal{S}x}(f,t)$,

$$S_{sx}(f,t) = E_T \frac{P_a(t)}{f\sqrt{2\pi\delta(t)}} \exp\left[-\frac{1}{2}\left(\frac{\ln f - \ln\beta(t)}{\delta(t)}\right)^2\right] \tag{15}$$

The discussion of using such a model to simulate the nonstationary ground motions is outside the scope of this study and could be found in [26,27].

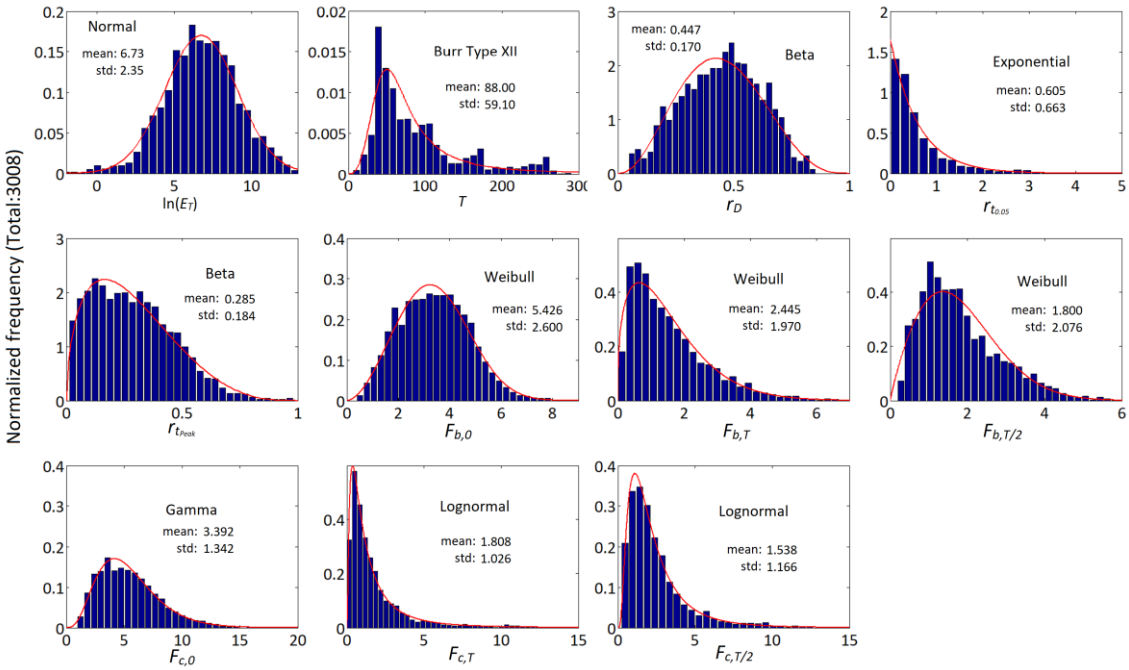

Fig. 4 – Normalized frequency diagrams of each parameter and the corresponding fitted probability distribution function

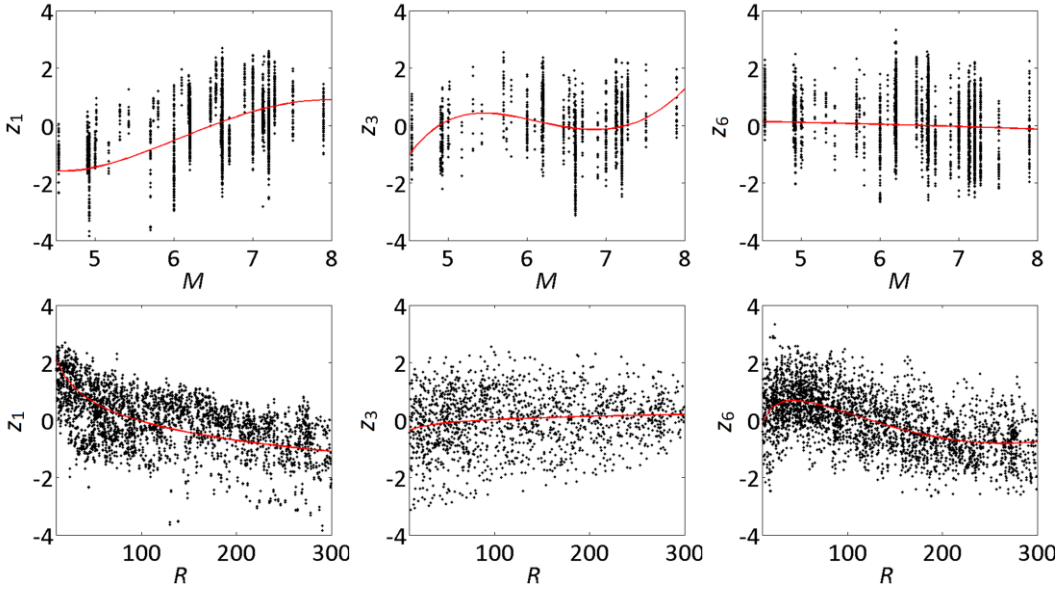

Fig. 5 – Parameters z_1, z_3 and z_6 VS M and R_{rup} and their fitted mean model.

5. Conclusion

The development of a model to represent the TFPSD function of nonstationary stochastic ground motions as functions of magnitude, rupture distance and shear wave velocity at the site is explored. The analysis of TFPSD function is based on the S-transform.

A preliminary probabilistic model of the time-frequency representation is developed based on the assessment of 1504 ground motion records, each with two horizontal components, selected from the NGA-West2 database. The model requires 11 model parameters. Empirical equations for these 11 model parameters as functions of magnitude, rupture distance and shear wave velocity are given.

It is observed that magnitude and rupture distance influences the model parameters significantly and the shear wave velocity has a less impact on the estimated model parameters The regression models for the 11 model parameters are treated as preliminary results and the inter- and intra-event effects are not assessed fully. This issue is currently dealt with in our ongoing research.

6. Acknowledgments

We gratefully acknowledge the financial support received from several agencies: the University of Western Ontario, the China Scholarship Council (No.201707980007, for XZC) and the National Science and Engineering Research Council of Canada (RGPIN-2016-04814, for HPH).

7. References

[1] Abrahamson, N. A., Silva, W. J., Kamai, R. (2014): Summary of the ASK14 ground motion relation for active crustal regions. *Earthquake Spectra*, **30**(3), 1025-1055.

[2] Boore, D. M., Stewart, J. P., Seyhan, E., Atkinson, G. M. (2014): NGA-West2 equations for predicting PGA, PGV, and 5% damped PSA for shallow crustal earthquakes. *Earthquake Spectra*, **30**(3), 1057-1085.

[3] Campbell, K. W., Bozorgnia, Y. (2014): NGA-West2 ground motion model for the average horizontal components of PGA, PGV, and 5% damped linear acceleration response spectra. *Earthquake Spectra*, **30**(3), 1087-1115.

[4] Chiou, B. S. J., Youngs, R. R. (2014): Update of the Chiou and Youngs NGA model for the average horizontal component of peak ground motion and response spectra. *Earthquake Spectra*, **30**(3), 1117-1153.

[5] Idriss, I. M. (2014): An NGA-West2 empirical model for estimating the horizontal spectral values generated by shallow crustal earthquakes. *Earthquake Spectra*, **30**(3), 1155-1177.

[6] Liu, T. J., Hong, H. P. (2015): Application of spatially correlated and coherent records of scenario event to estimate seismic loss of a portfolio of buildings. *Earthquake Spectra*, **31**(4), 2047-2068.

[7] Boore, D. M. (2009): Comparing stochastic point-source and finite-source ground-motion simulations: SMSIM and EXSIM. *Bulletin of the Seismological Society of America*, **99**(6), 3202-3216.

[8] Atkinson, G. M., Assatourians, K., Boore, D. M., Campbell, K., Motazedian, D. (2009): A guide to differences between stochastic point-source and stochastic finite-fault simulations. *Bulletin of the Seismological Society of America*, **99**(6), 3192-3201.

[9] Priestley, M. B. (1965): Evolutionary spectra and non-stationary processes. *Journal of the Royal Statistical Society: Series B* (*Methodological*), **27**(2), 204-229.

[10] Priestley, M. B. (1981): *Spectral analysis and time series: probability and mathematical statistics*. New York Academic Press

[11] Grigoriu, M., Ruiz, S. E., Rosenblueth, E. (1988): The Mexico earthquake of September 19, 1985—Nonstationary models of seismic ground acceleration. *Earthquake Spectra*, **4**(3), 551-568.

[12] Yeh, C. H., Wen, Y. K. (1990): Modeling of nonstationary ground motion and analysis of inelastic structural response. *Structural Safety*, **8**(1-4), 281-298.

[13] Alamilla, J., Esteva, L., García-Pérez, J., Diaz-Lopez, O. (2001): Simulating earthquake ground motion at a site, for given intensity and uncertain source location. *Journal of Seismology*, **5**(4), 475-485.

[14] Shinozuka, M., Deodatis, G. (1991): Simulation of stochastic processes by spectral representation. *Applied Mechanics Reviews* 191-204

[15] Sabetta, F., Pugliese, A. (1996): Estimation of response spectra and simulation of nonstationary earthquake ground motions. *Bulletin of the Seismological Society of America*, **86**(2), 337-352.

[16] Pousse, G., Bonilla, L. F., Cotton, F., Margerin, L. (2006): Nonstationary stochastic simulation of strong ground motion time histories including natural variability: Application to the K-net Japanese database. *Bulletin of the Seismological Society of America*, **96**(6), 2103-2117.

[17] Rezaeian, S., Der Kiureghian, A. (2008): A stochastic ground motion model with separable temporal and spectral nonstationarities. *Earthquake Engineering & Structural Dynamics*, **37**(13), 1565-1584.

[18] Rezaeian, S., Der Kiureghian, A. (2010): Simulation of synthetic ground motions for specified earthquake and site characteristics. *Earthquake Engineering & Structural Dynamics*, **39**(10), 1155-1180.

[19] Yamamoto, Y., Baker, J. W. (2013): Stochastic model for earthquake ground motion using wavelet packets. *Bulletin of the Seismological Society of America*, **103**(6), 3044-3056.

[20] Cohen, L. (1995): *Time-frequency analysis*, Prentice-Hall, New Jersey, U.S.

[21] Stockwell, R. G. (2007): A basis for efficient representation of the S-transform. *Digital Signal Processing*, **17**(1), 371-393.

[22] Stockwell, R. G., Mansinha, L., Lowe, R. P. (1996): Localization of the complex spectrum: the S transform. *IEEE transactions on signal processing*, **44**(4), 998-1001.

[23] Ancheta, T. D., Darragh, R. B., Stewart, J. P., Seyhan, E., Silva, W. J., Chiou, B. S. J., Kishida, T. (2014): NGA-West2 database. *Earthquake Spectra*, **30**(3), 989-1005.

[24] Code, U. B. (1997, April): *Uniform building code*. In International Conference of Building Officials, Whittier, CA.

[25] Pinnegar, C. R., Mansinha, L. (2003): The S-transform with windows of arbitrary and varying shape. *Geophysics*, **68**(1), 381-385.

[26] Hong, H. P., Cui, X.Z. (2019): Time-frequency spectral representation models to simulate nonstationary processes and their use to generate ground motions. Manuscript submitted to Journal of Engineering Mechanics.

[27] Cui, X. Z., Hong, H. P. (2020): Use of Discrete Orthonormal S Transform to Simulate Earthquake Ground Motions, *Bulletin of the Seismological Society of America*, doi: 10.1785/0120190212

[28] Trifunac, M. D., Brady, A. G. (1975): On correlation of seismoscope response with earthquake magnitude and Modified Mercalli Intensity. *Bulletin of the Seismological Society of America*, **65**(2), 307-321.

